







Thermolytic synthesis of cobalt and cobalt sulfide nanoparticles using Cobalt(II) N^O Schiff base complexes as single molecular precursors

Sandile H. KHOZA¹, Siphamandla C. MASIKANE¹, Sixberth MLOWE^{1,*},
Itegbeyogene P. EZEKIEL², Thomas MOYO², Neerish REVAPRASADU¹

¹Department of Chemistry, University of Zululand, KwaDlangezwa, South Africa

²School of Chemistry and Physics, University of KwaZulu-Natal, Westville Campus, Durban, South Africa

Received: 21.12.2017

Accepted/Published Online: 31.05.2018

Final Version: 11.10.2018

Abstract: Two novel N^O-type Schiff base ligands and the corresponding Co(II) complexes are reported. Thermogravimetric analysis indicated that the complexes are potential molecular precursors for the fabrication of cobalt and cobalt-containing nanomaterials. The significant difference in the thermal decomposition profiles is recognized as an influence of structural differences on the complexes. Thus, the complexes were thermally decomposed using the melt and hot injection methods to examine the properties of the obtained cobalt and cobalt sulfide nanoparticles, respectively. The reaction parameters employed during the fabrication processes, in addition to structural differences, influenced the morphological and crystallographic phases and magnetic properties of the synthesized nanoparticles. We have investigated the morphological properties and the crystallographic phase compositions of the nanoparticles by various electron microscopy and diffraction techniques, as well as energy-dispersive X-ray spectroscopy. The melt reactions produced phase-pure cobalt nanoparticles, which exhibit ferromagnetic behavior. The hot injection method utilized 1-dodecanethiol (DDT) as both sulfur source and capping agent. We indexed the DDT-capped cobalt sulfide nanoparticles to cubic Co₉S₈ and Co₃S₄ phases using powder X-ray diffraction, high-resolution transmission electron microscopy imaging, and selected area electron diffraction. The crystallite sizes for Co₉S₈ and Co₃S₄ nanoparticles, based on the Scherrer equation, were 12.4 nm and 14.1 nm, respectively. We find significant differences in the magnetic properties, attributed to nonmagnetic inclusions and vacancies due to the presence of S atoms.

Key words: Cobalt, cobalt sulfide, melt, 1-dodecanethiol, Schiff base

1. Introduction

Nanotechnology-based research fields have shown a drastic increase in the interest of various metal nanoparticles (MNPs) compared to their corresponding group V and VI counterparts. This trend is primarily due to their unique properties, which are relatively easy to harness. MNPs are interesting systems due to their high proportion of surface atoms, which offer increased active sites, and to their unique electronic properties at the limit between the molecular and metallic states.¹ Cobalt nanoparticles possess extraordinary high-density magnetic properties, hardness levels, sintering reactivities, and impact resistance properties.² These are desired properties in the field of data storage and biomedical applications. Thus, Co MNPs are potential candidates in this context. Other interesting features include multiple crystal structures, including the face-centered cubic, hexagonally closed packed, and ϵ -cobalt,² which show a strong correlation to their magnetic or electronic properties.

*Correspondence: sixb2809@gmail.com

The methods used to prepare cobalt nanoparticles have been studied broadly. They include thermal decomposition,^{3,4} gas vapor condensation,^{5,6} reduction of cobalt salt,^{7,8} and colloidal precipitation.⁹ Thermal decomposition is mostly preferred due to its cost effectiveness and upscaling capabilities. The method normally involves the decomposition of Co complexes such as cobalt carbonyl ($\text{Co}_2(\text{CO})_8$),¹⁰ bis(salicylidene)cobalt(II),¹¹ and bis(2-hydroxyacetophenato)cobalt(II)¹² to obtain the corresponding Co MNPs.

Transition metal sulfide nanoparticles have also attracted immense attention due to their rich structural diversities, which lead to unique electronic and magnetic properties.^{13,14} They have reported applications in solar cells, light-emitting diodes, sensors, thermoelectric devices, lithium-ion batteries, fuel cells, and nonvolatile memory devices.^{15–17} Cobalt sulfide is an intricate system that exists in many phases, such as CoS, CoS_2 , Co_2S_3 , Co_3S_4 , Co_4S_3 , and Co_9S_8 .^{18–20} Thus, to obtain a phase-pure material presents a challenge, since minor variations of the synthetic parameters could complicate the crystal phase of Co–S systems. The control of morphology is also difficult during the synthetic protocol because of the stoichiometry caused by the coexistence of strongly reducible cobalt and oxidizable sulfide ions.²¹ Nonetheless, cobalt sulfide nanoparticles have found use in many applications such as solar energy absorbers²² and ultradense magnetic recording.²³ An appropriate example is Co_9S_8 -based counter electrodes used in dye-sensitized solar cells, which collect electrons from an external circuit and speed up the reduction of I^{3-} for dye degradation.^{24–28} Its use in Li ion batteries is also widely reported.^{29–31}

To synthesize cobalt sulfide nanoparticles, different methods are available. Maneeprakorn et al.¹² demonstrated access to phase-pure Co_9S_8 nanoparticles through the solvothermal decomposition of di-*t*-butyldithiophosphinatocobalt(II) complex in the presence of tri-*n*-octylphosphine oxide and hexadecylamine at 300 °C.³² They also reported both phase and morphology transformations of cobalt sulfide nanoparticles through the same method, although different Co(II) thiobiuret complexes and long-chain amines were used as precursors and solvents, respectively.³³ These cobalt sulfide nanoparticles exhibited cubic and/or hexagonal phases, as well as various morphologies, including trigonal prisms, spheres, and hexagonally faceted crystal structures. Other solvothermal-based routes are reported elsewhere.^{34,35} Cobalt sulfide nanoparticles are also obtained from various methods such as the hydrothermal method,³⁶ pyrolysis,³⁷ and template-confined growth.³⁸

Schiff bases are compounds that are rarely reported as precursors for the fabrication of nanoparticles and nanomaterials. Schiff bases are generally used as chelating ligands because they are capable of forming stable complexes with metal ions.^{39,40} The complexes are widely exploited for their biochemical and antimicrobial activities. For example, Co(II) Schiff-base complexes are simplified models in the study of reversible binding of dioxygen in the field of pharmaceutical science.^{41–43} There are only a few reported articles on the synthesis of nanoparticles using Schiff base complexes as precursors.^{44,45}

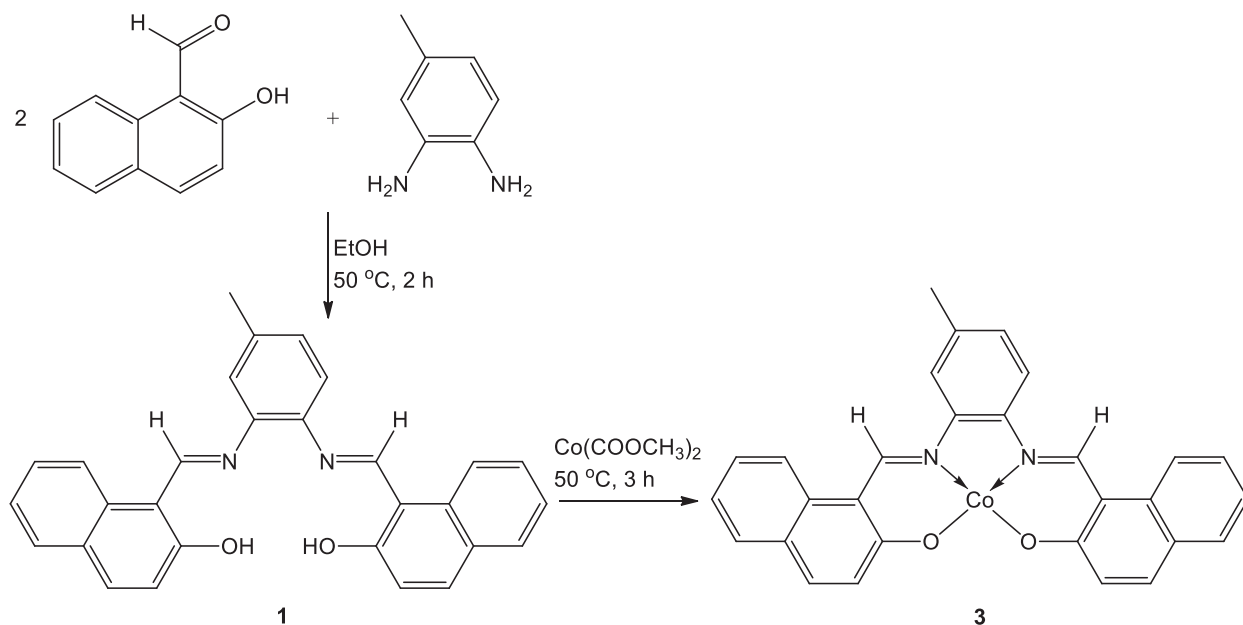
Herein, we report for the first time the synthesis and characterization of novel Co(II) Schiff base complexes. The report further demonstrates that the complexes are versatile molecular precursors in the fabrication of cobalt and cobalt sulfide nanoparticles. The former is achieved through a solventless melt method, while the latter focuses on a one-pot solvothermal method using 1-dodecanethiol as both sulfur source and capping agent.

2. Results and discussion

2.1. Characterization of the precursor

Schiff base ligands **1** and **2**, obtained through the condensation reaction of the appropriate aldehyde with 4-methylorthophenylenediamine, were isolated in good yields as orange crystals from the slow evaporation of the

methanolic solutions. The ligands could easily form complexes with Co(II), thus yielding complexes **3** (Scheme 1) and **4** (Scheme S1), respectively. The complexes precipitated as analytically pure brown crystalline solids directly from the reactions, without need of recrystallization. Microanalysis determined the purity of the synthesized compounds. Nuclear magnetic resonance (NMR) and Fourier transform infrared (FT-IR) spectroscopy provided structural elucidation.



Scheme 1. Preparation of *N,N'*-bis(1-naphthaldehyde)-4-methyl-2,6-diaminophenol **1** and the corresponding Co(II) complex **3**.

The ^1H NMR spectral identification of methoxy, methyl, and azomethine protons for ligand **1** are singlet peaks observed at 2.4, 9.7, and 15.2 ppm, respectively. The aromatic protons appeared in the range of 6.98–7.39 ppm as a multiplet peak and the protons of the hydroxyl group on the phenol moieties occurred at 15.2 ppm as a singlet peak. For ligand **2**, the methoxy, methyl, and azomethine protons observed at 3.86, 2.57, and 8.92 ppm, respectively, are singlet peaks. The multiplet peak arising from the aromatic protons appeared in the same region as for ligand **1**, while the hydroxyl proton observed at 12.46 ppm is singlet. The downfield shift of the hydroxyl proton may be due to strong internal hydrogen bonding.⁴⁶

The IR spectra show a shift from 1539–1560 cm^{-1} in ligand **1** (Figure S1a) to 1541–1575 cm^{-1} in complex **3** (Figure S1b), indicative of the azomethine nitrogen interacting with the metal ion.^{47–50} The two new bands appearing in the low-frequency region of complex **3** at 570 cm^{-1} and 480 cm^{-1} are typical of $\nu_{\text{Co}-\text{O}}$ and $\nu_{\text{Co}-\text{N}}$ frequencies, respectively.^{50,51} Similar observations were made between the spectra of ligand **2** (Figure S2a) and complex **4** (Figure S2b); shifts of the $\nu_{(\text{C}=\text{N})}$ and $\nu_{(\text{C}-\text{O})}$ bands from 1621 cm^{-1} to 1654 cm^{-1} and 1329 cm^{-1} to 1359 cm^{-1} , respectively, were observed. The $\nu_{\text{Co}-\text{O}}$ and $\nu_{\text{Co}-\text{N}}$ bands appeared at 552 cm^{-1} and 456 cm^{-1} , respectively.

Thermogravimetric (TGA) and differential scanning calorimetry (DSC) analyses can determine the thermal stability of the complexes. The TGA profile of complex **3** (Figure S3) shows a single-step decomposition at 420 °C, corroborated by the exothermic peak observed at the same temperature in the DSC plot (Figure

S3). Although the complex is thermally stable in the 25 °C to 410 °C region, the DSC plot shows a series of physical phase transformations. The TGA profile for complex **4** (Figure S4) shows a three-step decomposition pattern. The first decomposition step in the 100–110 °C region accounts for the 7% weight loss of water vapors. A second sharp step at around 350 °C is due to the decomposition of volatile organic moiety. The DSC plot (Figure S4) showed three exothermic peaks, which coincide with the decompositions occurring at 80 °C, 350 °C, and 820 °C. Furthermore, physical phase transformation occurs in the 140 °C to 160 °C region.⁵²

2.2. Synthesis of cobalt nanoparticles by the melt method

The protocols used in the melt reactions mimic that of the TGA, i.e. decomposition under inert N₂ atmosphere. The reactions occurred at 450 °C, a temperature slightly above that of the decomposition for complexes **3** and **4** (Figures S3 and S4, respectively). The reaction lasted for an hour, prior to cooling the furnace to room temperature under N₂. At the specified temperature, the complexes displayed the true meaning of a single source precursor and provided self-capping upon decomposition, thus yielding cubic nanoparticles with an average particle size of 30 ± 5 nm (Figure 1a) for particles obtained from complex **3**, and an average size of 14 ± 4 nm (Figure 1b) for complex **4**. The histograms of particle size distribution (Figures 1c and 1d) exhibit fairly narrow size distribution. The powder X-ray diffraction (p-XRD) patterns (Figure 2) of the nanoparticles from both complexes concur with the reflections of cubic Co (PDF card no. 00-015-0608). Three distinct diffraction peaks observed at 2θ values of 44.2°, 51.5°, and 75.9° corresponded to the (111), (200), and (200) planes, respectively. The method is considered self-efficient, i.e. the cubic shape of the nanoparticles coincides with the cubic crystal structure in the absence of solvents, which are normally employed to achieve this through minimizing surface tension resulting from contributing factors such as large van der Waal forces. Oxidation resulting from the exposure to air is common among challenges experienced in pursuit of preparing stable Co nanoparticles.¹¹ Our route, however, guarantees stability of the Co nanoparticles at ambient conditions.

2.3. Synthesis of cobalt sulfide nanoparticles by the thermolysis method

The optimum temperature and time conditions to obtain acceptable quality nanoparticles from the dual-source, one-pot hot injection method appear to be 270 °C and 4 h, respectively. The complexes and DDT are molecular precursors that release Co and S ions through decompositions pathways at elevated temperatures, thus yielding the corresponding cobalt sulfide material. The transmission electron microscope (TEM) images of the nanoparticles obtained from both complexes show signs characteristic of agglomeration (Figures 3a and 3b), thus presenting a challenge to conclude anything regarding monodispersity and morphological features. The high-resolution TEM (HR-TEM) image of the nanoparticles obtained from complex **3** (Figure 3c) shows well-defined lattice fringes calculated to be 2.94 Å and 1.73 Å, corresponding to the (311) and (440) planes of Co₉S₈ phase (ICDD 01-073-6395), respectively. The poor quality of the HR-TEM image for the nanoparticles obtained from complex **4** (Figure 3d) shows small lattice fringes, which results in difficulties measuring the lattice spacing. The selected area electron diffraction patterns were able to provide clear crystallographic features of the nanoparticles. The diffraction rings of the nanoparticles obtained from complex **3** (Figure 3e) were indexed to the (311) and (440) planes of the Co₉S₈ phase (ICDD 01-073-6395). Nanoparticles from complex **4** (Figure 3f) show three distinct diffraction rings, which are indexed to the (311), (440), and (400) planes of the Co₃S₄ phase (ICDD 00-047-1738).

The scanning electron microscope (SEM) images show the surface morphology of nearly spherical nanopar-

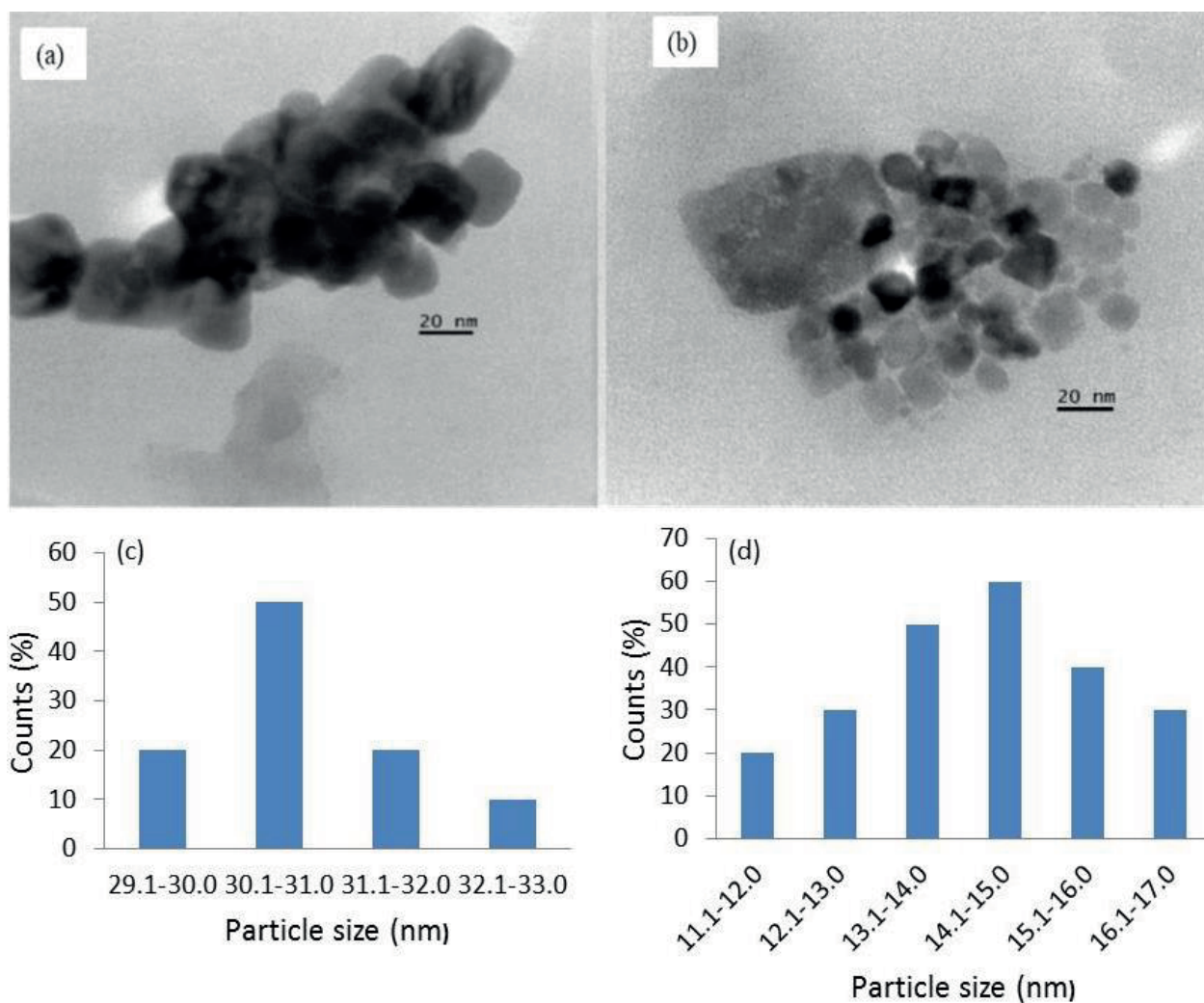


Figure 1. TEM images of cobalt nanoparticles prepared by melt of complex **3** (a) and complex **4** (b) at 450 °C for 1 h; (c) and (d) represent histograms of particle size distributions corresponding to the TEM images of (a) and (b), respectively.

ticles, which agglomerate to structures exhibiting an average diameter of between 100 nm to 600 nm (Figures 4a and 4b). The energy-dispersive X-ray (EDX) spectra show atomic compositions of 46.2% for Co and 53.8% for S for nanoparticles obtained from complex **3** (Figure 4c). Compositions of 42.3% for Co and 57.7% for S are obtained from complex **4** (Figure 4d).

Figure 5 shows the p-XRD patterns of the prepared cobalt sulfide nanoparticles obtained using complex **3** (Figure 5a) and complex **4** (Figure 5b). The reflection peaks in the p-XRD pattern of the nanoparticles obtained from complex **3** were consistent with the reported values of bulk Co_9S_8 (cobalt pentlandite) (ICDD 01-073-6395), while those from complex **4** were indexed to cubic Co_3S_4 phase (ICDD 00-047-1738). Both patterns show no additional peaks that would suggest impurities, which indicates the phase purity of the product. Phase identification was confirmed further through atomic compositions obtained from EDX spectroscopy analysis. The EDX spectrum of the nanoparticles obtained from complex **3** suggests a sulfur-rich Co_9S_8 phase, with experimental compositions of 46.2% for Co and 53.8% for S having shifted from the theoretical composition of

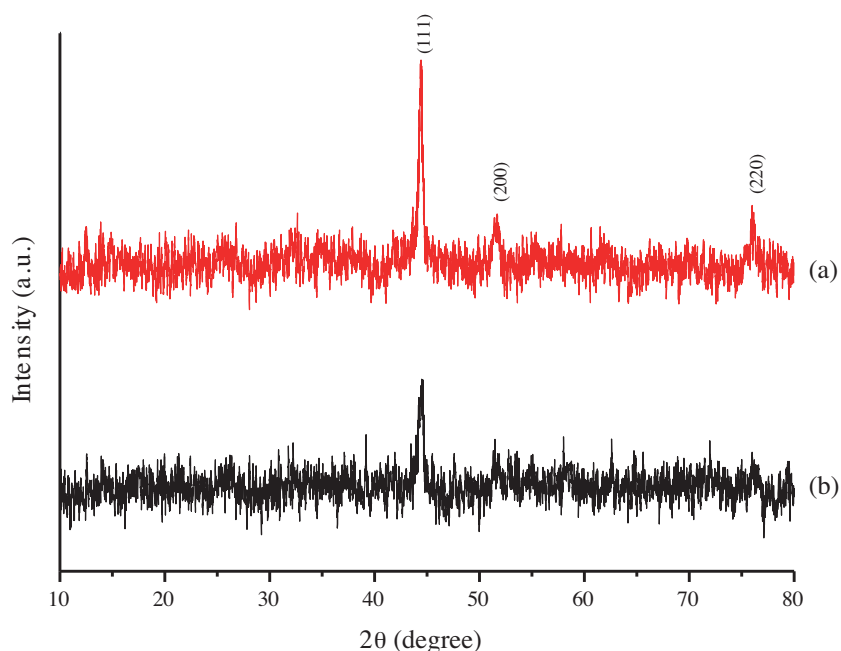


Figure 2. The p-XRD patterns of Co (PDF card no. 00-015-0608) nanoparticles prepared by melt reaction of (a) complex **3** and (b) complex **4** at 450 °C for 1 h.

52.9% for Co and 47.1% for S (Figure 4c). Nanoparticles from complex **4** exhibit atomic compositions of 42.3% Co and 57.7% S, corresponding to 42.8% Co and 57.2% S theoretical values for Co_3S_4 (Figure 4d).

Although the particle sizes could not be measured from the imaging techniques, the crystallite sizes of both Co_9S_8 and Co_3S_4 nanoparticles were then estimated by the Scherrer formula reported elsewhere and were 12.44 nm and 14.10 nm, respectively.^{53,54} Here the synthesis temperature is lower: 270 °C compared to 450 °C for cobalt nanoparticles produced by the melt method (section 3.2). For synthesis at 450 °C, the particle size is higher for complex **3** and no significant change is observed for complex **4**. Increased synthesis temperature or thermal annealing at higher temperature is normally associated with increased particle sizes.⁵⁵ In the present case, complex **4** appears to have higher thermal stability, indicated by the lack of change in particle size from 270 °C to 450 °C.

2.4. Magnetic properties

Magnetic properties can offer useful information that is helpful in the understanding of the basics of nanomagnetism. The magnetization depends on different parameters such as constituent atoms, microstructure, shape, temperature, magnetic fields, and particle sizes and microstructures of the materials.⁵⁶ The magnetization measured at room temperature for cobalt nanoparticles obtained from complexes **3** and **4** appear to show ferromagnetic behavior (Figures 6–8). The approach to saturation of the initial magnetization curves in Figure 8 were determined in high fields $H > 2000$ Oe using the empirical formula⁵⁷ for ferromagnets of the form

$$M(H) = M_S \left(1 - \frac{a_1}{H} - \frac{a_2}{H^2} \right) + \chi_{hf} H, \quad (1)$$

where a_1 and a_2 are constants, M_S is the spontaneous magnetization, and χ_{hf} is the high field susceptibility. We attribute the term a_1/H to structural defects or nonmagnetic inclusions, which we assume would exist in

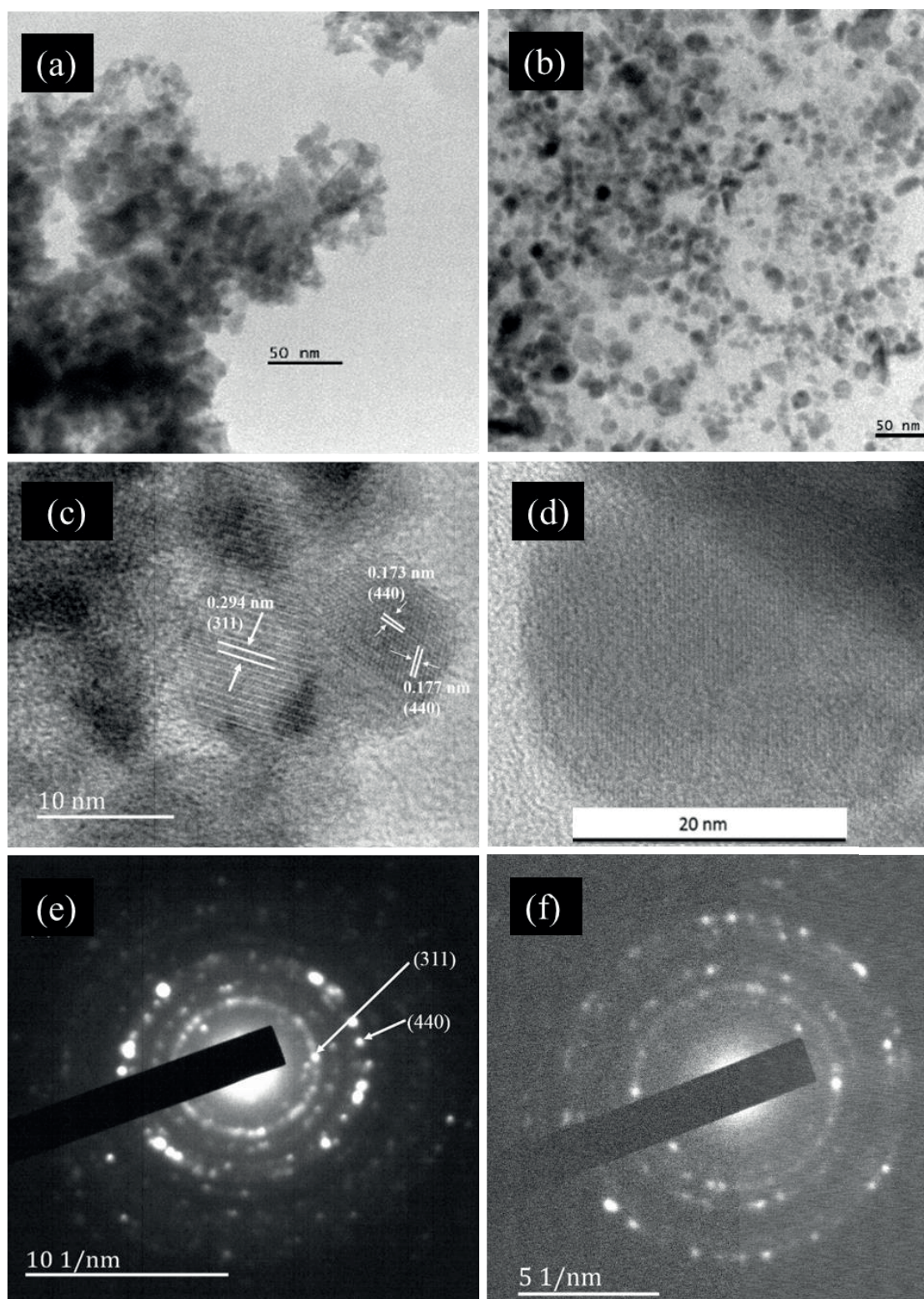


Figure 3. TEM images (a, b), HR-TEM images (c, d), and SAED patterns (e, f) of cobalt sulfide nanoparticles prepared from complex **3** and complex **4**, respectively, at 270 °C for 4 h.

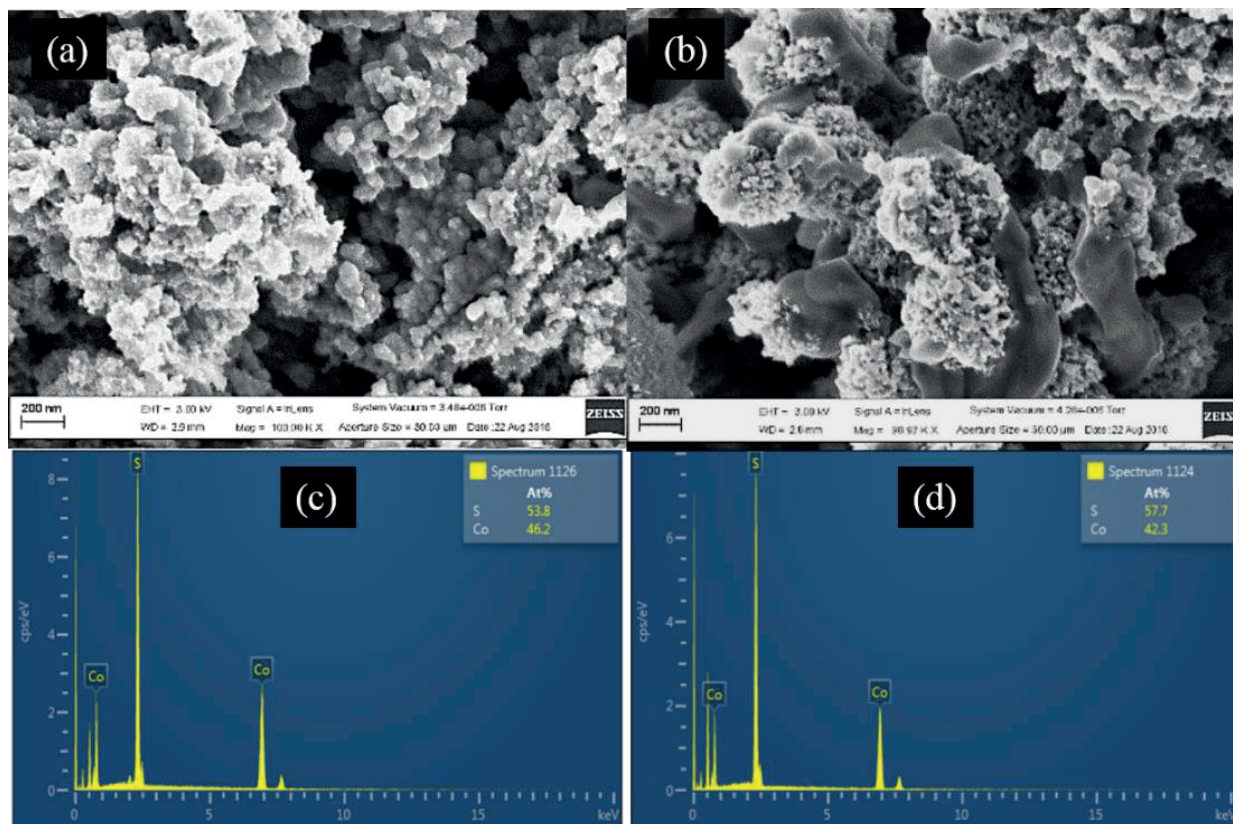


Figure 4. SEM images (a, b) and EDX patterns (c, d) of cobalt nanoparticles prepared from (a,c) complex **3** and (b, d) complex **4** at 270 °C for 4 h.

the present set of nanomaterials. The cause of a_2/H^2 term is uniform magneto-crystalline anisotropy. When this term is included in the fits in Figure 8, it does not give realistic a_2 values. Hence, we assumed $a_2 \approx 0$ in the present case. The Table shows a summary of the results based on the empirical fits and hysteresis loop measurements. The Table shows significant differences between complexes **3** and **4** parameters. In the Stoner–Wohlfarth theory,⁵⁸ H_C is related to the anisotropy constant (K) and the spontaneous magnetization M_S by

Table. Parameters derived from magnetization measurements for complexes **3** and **4**.

Parameters	Complex 3	Complex 4
χ^2	0.99961	0.99801
M_S (emu/g)	3.04 ± 0.02	5.38 ± 0.12
a_1 (Oe)	907 ± 12	1146 ± 34
a_2 (Oe ²)	0	0
χ_{hf} (emu g ⁻¹ Oe ⁻¹)	$(1.80 \pm 0.02) \times 10^{-4}$	$(4.90 \pm 0.09) \times 10^{-4}$
H_C (Oe)	130 ± 1	150 ± 1
M_r (emu/g)	0.21 ± 0.01	0.41 ± 0.01
$H_C M_S$ (Oe emu/g)	395 ± 4	807 ± 19
K (Oe emu/g)	411 ± 4	841 ± 20

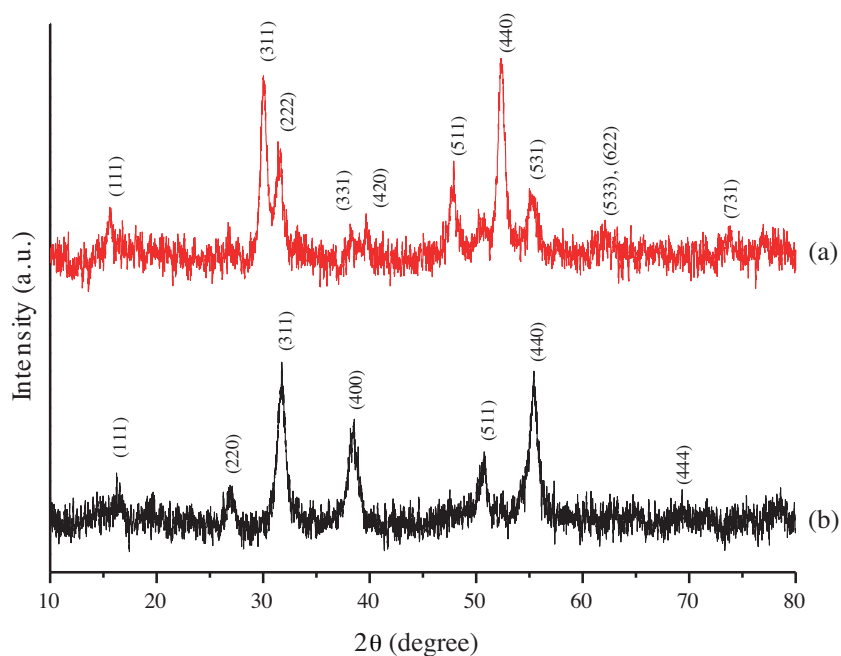


Figure 5. The p-XRD patterns of nanoparticles prepared from (a) complex **3** and (b) complex **4** at 270 °C for 4 h, indexed to Co_9S_8 (ICDD no. 01-073-6395) and Co_3S_4 (ICDD no. 00-047-1738), respectively.

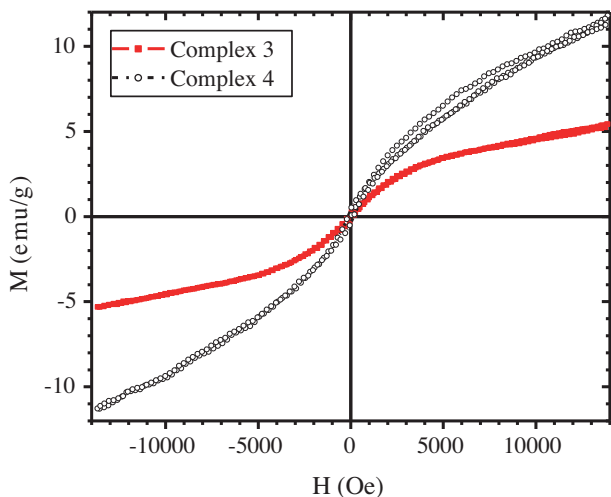


Figure 6. Hysteresis loop of cobalt nanoparticles prepared by pyrolysis of complex **3** and complex **4** at 450 °C for 1 h.

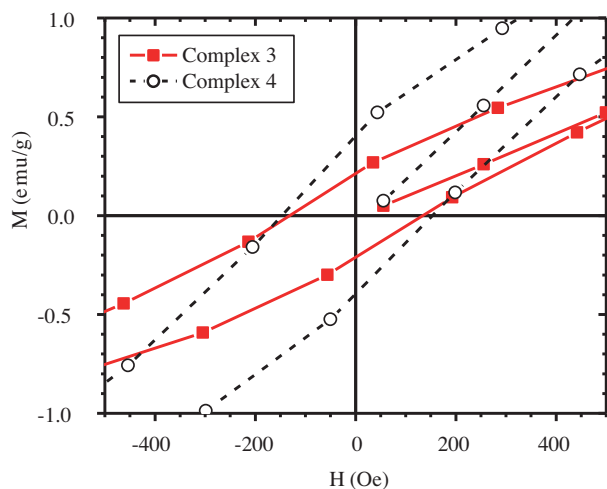


Figure 7. Hysteresis loops in low magnetic fields for complexes **3** and **4**.

$$H_C = \frac{0.96K}{M_S}. \quad (2)$$

We find the anisotropy constant for complex **4** to be approximately double that of complex **3**. Based on the EDX spectra in Figure 4d, complex **4** has higher S content than complex **3** (57.7% and 46.2%, respectively). Hence, we can expect a higher proportion of nonmagnetic inclusions in complex **4** to account for a higher coercive field and anisotropy, as expected from magnetization measurements.

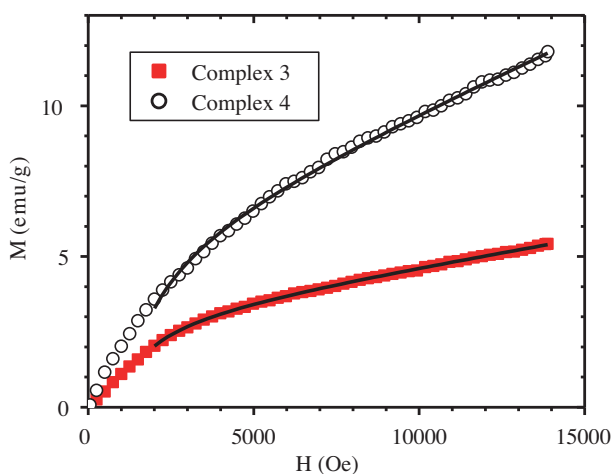


Figure 8. Initial magnetization curves for complexes **3** and **4** fitted by the empirical law of approach to saturation.

In conclusion, the work demonstrates that novel Co(II) Schiff base complexes are versatile molecular precursors for the fabrication of cobalt and cobalt sulfide nanoparticles. The melt and hot injection methods offer access to cost-efficient and easily modifiable routes, respectively. This allows fine-tuning of the nanoparticles' properties. Phase-pure cobalt nanoparticles obtained by the melt method at a reaction temperature as low as 450 °C exhibited ferromagnetic behavior, indicating possibility for applications in magnetic fields. The one-pot hot injection method produced cobalt sulfide nanoparticles of different crystallographic phases, mainly due to the structural differences of the precursors. We suspect that Co_3S_4 has higher anisotropy and thermodynamic stability than Co_9S_8 .

3. Experimental

3.1. Materials

All reagents and solvents were of analytical/spectroscopic grades and used without further purification. These included tri-*n*-octylphosphine, 1-dodecanethiol (DDT), 2-hydroxy-1-naphthaldehyde, Co(II) acetate, 4-methyl-*o*-phenyldiamin, 2-hydroxy-5-methoxybenzaldehyde, and triethylamine from Sigma-Aldrich (St. Louis, MO, USA), while ethanol and methanol solvents were from Merck, South Africa.

3.2. Characterization

A PerkinElmer automated model 2400 series II CHNS/O analyzer performed elemental (CHN) microanalysis (Waltham, MA, USA). A Bruker FT-IR tensor 27 spectrophotometer, equipped with a standard ATR crystal cell detector in the wavenumber range 200–4000 cm^{-1} , recorded the IR spectra (Billerica, MA, USA). A PerkinElmer Pyris 6 TGA equipped with a closed perforated ceramic pan determined the thermal properties of the complexes at a heating rate of 20 °C/min from 30 °C to 800 °C under N_2 gas flow rate of 10 mL/min. A Bruker Advance III 400 MHz spectrophotometer equipped with trimethylsilane as an internal standard reference recorded the proton nuclear magnetic resonance (^1H NMR) spectra of both the Schiff base ligands and metal complexes.

A JEOL 1400 TEM at an accelerating voltage of 120 kV and a JEOL 2010 HR-TEM at an accelerating voltage of 200 kV were used to characterize the morphology and particle sizes of the cobalt nanoparticles (Tokyo,

Japan). Samples were prepared on copper grids by evaporating drops of nanoparticle suspensions in ethanol. The images were captured using iTEM software from a Megaview III camera (Emsis, Münster, Germany). A Zeiss Ultra Plus FEG SEM (Oberkochen, Germany) was used for surface morphology analysis, equipped with an Oxford detector EDX at 20 kV, which uses Aztec software (Springfield, NJ, USA) for elemental analysis. p-XRD patterns of the nanoparticles were recorded at room temperature in the angle 2θ range (20–80°) using an Advanced Bruker AXS D8 diffractometer, equipped with nickel-filtered Cu K_α radiation ($\lambda = 1.542 \text{ \AA}$) at 40 kV and 40 mA.

The magnetic properties of the samples were determined from magnetization measurement at room temperature on a Lakeshore model 735 vibrating sample magnetometer (Westerville, OH, USA). This involved measurements of initial magnetization curves and hysteresis loops in magnetic fields up to about 14 kOe.

3.3. Synthesis of Schiff base ligands and cobalt complexes

3.3.1. Synthesis of *N,N'*-bis(1-naphthaldehyde)-4-methylorthophenylenediimine **1**

Schiff base ligand **1** was prepared by the condensation reaction of 2-hydroxy-1-naphthaldehyde (6.91 g, 40.0 mmol) with 4-methylorthophenylenediimine (2.47 g, 20.0 mmol) in 75 mL of ethanol. We heated the reactants while stirring at 50 °C for 2 h, separated the precipitate from the hot mixture by filtration, recrystallized it from methanol, dried the precipitate under vacuum, and stored it in a desiccator.

Yield: 80.4%; $^1\text{H NMR}$ (400 MHz, DMSO- d_6 , δ /ppm): 15.2 (2H, s, O–H), 9.7 (2H, s, –N=CH), 6.9–8.1 (9H, m, aromatic), 2.4 (3H, s, –CH₃), 8.4–8.7 (6H, s, –OCH₃); IR (ATR, cm^{-1}): 1619 (–C=N stretching of azomethine group), 1329 (–C–O stretching of phenolic group); Anal. Calcd. for C₂₉H₂₂N₂O₂: C, 80.91; H, 5.15; N, 6.51. Found: C, 79.83; H, 4.76; N, 6.22.

3.3.2. Synthesis of *N,N'*-bis (5-methoxybenzaldehyde)-4-methylorthophenylenediimine **2**

The same reaction protocol for **1** with minor modifications. We used 5-methoxybenzaldehyde (2.72 g, 20.0 mmol) and 4-methylorthophenylenediimine (1.24 g, 10.0 mmol).

Yield: 87.5%; $^1\text{H NMR}$ (400 MHz, DMSO- d_6 , δ /ppm): 12.46 (2H, s, O–H), 8.92 (2H, s, –N=CH), 6.98–7.39 (9H, m, aromatic), 2.57 (3H, s, –CH₃), 3.86 (6H, s, –OCH₃); IR (ATR, cm^{-1}): 1621 (–C=N stretching of azomethine group), 1334 (–C–O stretching of phenolic group); Anal. Calcd. for C₂₃H₂₂N₂O₄: C, 70.75; H, 5.68; N, 7.17. Found: C, 70.51; H, 5.70; N, 6.88.

3.3.3. Synthesis of *N,N'*-bis (1-naphthaldehyde)-4-methylorthophenylenediiminatocobalt(II) complex **3**

A solution of Co(II) acetate (750 mg, 3.00 mmol) in 50 mL of methanol was added dropwise to the solution of the Schiff base ligand **1** (1.18 g, 3.00 mmol) in 90 mL of methanol. Refluxing and stirring of the mixture were maintained at 50 °C for 3 h. On cooling, the brown precipitate required filtration and washing several times with methanol. The final product was vacuum dried.

Yield: 83.7%; IR (ATR, cm^{-1}): 1583 (–C=N stretching of azomethine group), 1360 (–C–O stretching of phenolic group) 554 (Co–O), 458 (Co–N stretching); Anal. Calcd. for C₂₉H₂₀N₂O₂Co: C, 71.46; H, 4.14; N, 5.75. Found: C, 70.89; H, 4.40; N, 6.05.

3.3.4. Synthesis of *N, N'*-bis(5-methoxybenzaldehyde)-4-methylorthophenylenediiminatocobalt(II) complex **4**

The reaction protocol for **3** was followed with minor modifications. Co(II) acetate (750 mg, 3.00 mmol), the Schiff base ligand (**2**) (1.18 g, 3.00 mmol), and triethylamine (610 mg, 6 mmol) were used.

Yield: 72.4%; IR (ATR, cm^{-1}): 1588 (-C=N stretching of azomethine group), 1364 (-C-O stretching of phenolic group) 552 (Co-O), 456 (Co-N stretching); Anal. Calcd. for $\text{C}_{23}\text{H}_{20}\text{N}_2\text{O}_4\text{Co}$: C, 61.75; H, 4.51; N, 6.26. Found: C, 61.48; H, 4.70; N, 6.05.

3.3.5. Synthesis of cobalt nanoparticles by melt method in a furnace

In a typical reaction, 100 mg of the complex is transferred into a 1×2 ($l \times b$ in cm) ceramic boat which is then placed in a glass tube connected to a N_2 line. Subsequently, the tube is inserted into an electric furnace, and gradually heated to 450°C under the constant flow of nitrogen gas for 1 h. Before removing the tube, the furnace is cooled to room temperature and a black residue is collected for further analyses.

3.3.6. Synthesis of cobalt sulfide nanoparticles by thermolysis

The cobalt sulfide nanoparticles were synthesized by solvothermal decomposition of complexes **3** and **4** in DDT following reaction protocols reported elsewhere.⁵⁹ Briefly, 200 mg of each Co(II) Schiff base complex was dissolved in tri-*n*-octylphosphine (6.0 mL) to produce a dark purple solution, which was then injected into preheated DDT (6.00 g) at 270°C in a three-neck flask equipped with a condenser and thermometer. The solution turned black and its temperature decreased. After the solution stabilized back to 270°C , it was stirred for an additional 4 h, after which the solution was cooled to about 70°C and excess methanol added to induce a reversible flocculation of the nanoparticles. The black flocculate was separated from the supernatant via centrifugation. We repeated the washing of the flocculate using excess methanol three times. The resultant Co nanoparticles were dissolved in toluene for characterization.

Acknowledgment

The authors thank the National Research Foundation (NRF) South Africa through the South African Research Chair Initiative (SARChI) for their financial support (Grant number 64820).

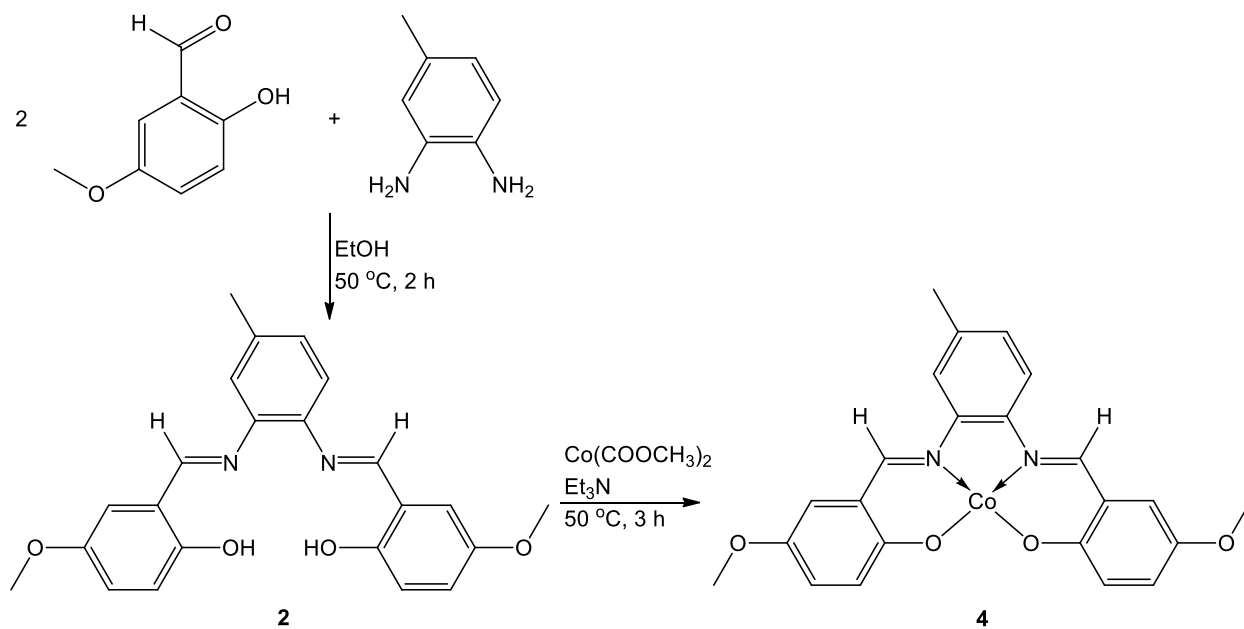
References

1. Trindade, T.; O'Brien, P.; Pickett, N. L. *Chem. Mater.* **2001**, *13*, 3843-3858.
2. Connolly, J.; St. Pierre, T. G.; Rutnakornpituk, M.; Riffle, J. S. *J. Phys. D. Appl. Phys.* **2004**, *37*, 2475-2482.
3. Puentes, F. V.; Krishnam, M. K.; Alivisatos, P. A. *Science* **2001**, *291*, 2115-2117.
4. Murray, C. B.; Sun, S.; Gaschler, W. *IBM J. Res. Dev.* **2001**, *45*, 47-56.
5. Dong, X. L.; Choi, C. J.; Kim, B. K. *Scripta Mater.* **2002**, *47*, 857-861.
6. Wang, Z. H.; Choi, C. J.; Kim, B. K.; Zhang, Z. D. *J. Alloys Compd.* **2003**, *351*, 319-323.
7. Sun, S.; Murray, C. B. *J. Appl. Phys.* **1999**, *85*, 4325-4330.
8. Luna, C.; Morales, M. P.; Serna, C. J.; Vazquez, M. *Mater. Sci. Eng. C* **2003**, *23*, 1129-1132.
9. Ichiyanagi, Y.; Yamada, S. *Polyhedron* **2005**, *24*, 2813-2816.
10. Shukla, N.; Svedberg, E. B.; Ell, J.; Roy, A. J. *Mater. Lett.* **2006**, *60*, 1950-1955.

11. Salavati-Niasari, M.; Davar, F.; Mazaheri, M.; Shaterian, M. *J. Magn. Magn. Mater.* **2008**, *320*, 575-578.
12. Maneerprakorn, W.; Malik, A. M.; O'Brien, P. *J. Mater. Chem.* **2010**, *20*, 2329-2335.
13. Ramasamy, K.; Malik, M. A.; Revaprasadu, N.; O'Brien, P. *Chem. Mater.* **2013**, *25*, 3551-3569.
14. Lai, C. H.; Lu, M. Y.; Chen, L. J. *J. Mater. Chem.* **2012**, *22*, 19-30.
15. Wu, Y.; Wadia, C.; Ma, W. L.; Sadtler, B.; Alivisatos, A. P. *Nano Lett.* **2008**, *8*, 2551-2555.
16. Li, T. L.; Lee, Y. L.; Teng, H. S. *J. Mater. Chem.* **2011**, *21*, 5089-5098.
17. Bierman, M. J.; Jin, S. *Energy Environ. Sci.* **2009**, *2*, 1050-1059.
18. Chen, X. Y.; Zhang, Z. J.; Qiu, Z. G.; Shi, C. W.; Li, X. L. *J. Colloid Interface Sci.* **2007**, *308*, 271-275.
19. Wold, A.; Dwight, K. *Solid State Chemistry*; Chapman and Hall: New York, NY, USA, 1993.
20. Rao, C. N. R.; Pisharody, K. P. R. *Prog. Solid State Chem.* **1976**, *10*, 207-270.
21. Bao, S.; Li, Y.; Li, C. M.; Bao, Q.; Lu, Q.; Guo, J. *Cryst. Growth Des.* **2008**, *8*, 3745-3749.
22. Smith, G. B.; Ignatiev, A.; Zajac, G. *J. Appl. Phys.* **1980**, *51*, 4186-4196.
23. Whitney, T. M.; Jiang, J. S.; Searson, P.; Chien, C. *Science* **1993**, *261*, 1316-1319.
24. Wang, G.; Zhuo, S. *Phys. Chem. Chem. Phys.* **2013**, *15*, 13801-13804.
25. Tai, S. Y.; Chang, C. F.; Liu, W. C.; Liao, J. H.; Lin, J. Y. *Electrochim. Acta* **2013**, *107*, 66-70.
26. Faber, M. S.; Park, K.; Cabán-Acevedo, M.; Santra, P. K.; Jin, S. *J. Phys. Chem. Lett.* **2013**, *4*, 1843-1849.
27. Kung, C. W.; Chen, H. W.; Lin, C. Y.; Huang, K. C.; Vittal, R.; Ho, K. C. *ACS Nano.* **2012**, *6*, 7016-7025.
28. Chen, H. W.; Kung, C. W.; Tseng, C. M.; Wei, T. C.; Sakai, N.; Morita, S.; Ikegami, M.; Miyasaka, T.; Ho, K. C. *J. Mater. Chem. A* **2013**, *1*, 13759-13768.
29. Yue, G. H.; Yan, P. X.; Fan, X. Y.; Wang, M. X.; Qu, D. M.; Wu, Z. G.; Li, C.; Yan, D. *Electrochem. Solid State Lett.* **2007**, *10*, D29-D31.
30. Wang, Q.; Jiao, L.; Han, Y.; Du, H.; Peng, W.; Huan, Q.; Song, D.; Si, Y.; Wang, Y.; Yuan, H. *J. Phys. Chem. C* **2011**, *115*, 8300-8304.
31. Zhou, Y. X.; Yao, H. B.; Wang, Y.; Liu, H. L.; Gao, M. R.; Shen, P. K.; Yu, S. H. *Chem. Eur. J.* **2010**, *16*, 12000-12007.
32. Maneerprakorn, W.; Malik, M. A.; O'Brien, P. *J. Mater. Chem.* **2010**, *20*, 2329-2335.
33. Ramasamy, K.; Maneerprakorn, W.; Malik, M. A.; O'Brien, P. *Phil. Trans. R. Soc. A* **2010**, *368*, 4249-4260.
34. Kumar, N.; Raman, N.; Sundaresan, A. *Anorg. Allg. Chem.* **2014**, *640*, 1069-1074.
35. Pawar, A. S.; Garje, S. S. *Bull. Mater. Sci.* **2015**, *38*, 1843-1850.
36. Bornside, D. E.; Macosko, C. W.; Scriven, L. E. *J. Imaging Technol.* **1987**, *13*, 122-130.
37. Pengfei, Y.; Lili, S.; Xiangyu, H.; Chuanhui, X.; Haiying, W.; Feng, W. *Rare Metal Mater. Eng.* **2016**, *45*, 1700-1704.
38. Wirtz, M.; Martin, C. R. *Adv. Mater.* **2003**, *15*, 455-458.
39. Johnson, C. P.; Atwood, J. L.; Steed, J. W.; Bauer, C. B.; Rogers, R. D. *Inorg. Chem.* **1996**, *35*, 2602-2610.
40. Alizadeh, N.; Ershad, S.; Naeimi, H.; Sharghi, H.; Shamsipur, M. *Pol. J. Chem.* **1999**, *73*, 915-925.
41. Thangadurai, T. D.; Gowri, M.; Natarajan, K. *Synth. React. Inorg. Met. Org. Chem.* **2002**, *32*, 329-343.
42. Pui, A. *Croatica Chem. Acta* **2002**, *75*, 165-173.
43. Casella, L.; Gullotti, M. *Inorg. Chem.* **1986**, *25*, 1293-1303.
44. Aazam, E. S.; El-Said, W. A. *Bioorganic Chem.* **2014**, *57*, 5-12.
45. Parsaee, Z.; Mohammadi, K.; Ghahramaninezhad, M.; Hosseinzadeh, B. *New J. Chem.* **2016**, *40*, 10569-10583.

46. Bu, X. R.; Jackson, C. R.; Derveer, D. V.; You, X. Z.; Meng, Q. J.; Wang, R. X. *Polyhedron* **1997**, *16*, 2991-3001.
47. Kolawole, G. A.; Patel, K. S. *J. Chem. Soc., Dalton Trans.* **1981**, 1241-1245.
48. Patel, K. S.; Kolawole, G. A.; Earnshaw, A. *J. Inorg. Nucl. Chem.* **1981**, *43*, 3107-3112.
49. Osowole, A. A.; Kolawole, G. A.; Fagade, O. E. *Synth. React. Inorg. Met. Org. Chem.* **2005**, *35*, 829-836.
50. Nejo, A. A.; Kolawole, G. A.; Nejo, A. O. *J. Coord. Chem.* **2010**, *63*, 4398-4410.
51. Abd-Elza, M. M.; *J. Chin. Chem. Soc.* **2001**, *48*, 153-158.
52. Lee, C. H.; Hsu, C. K.; Chan, C. L. *Thermochim. Acta* **2002**, *392*, 173-176.
53. Scherrer, P. *Nachr. Ges. Wiss. Göttingen Math. Phys. Kl.* **1918**, *26*, 98-100.
54. Abdallah, H. M. I.; Moyo, T.; Ezekiel, I. P.; Osman, N. S. E. *J. Magn. Magn. Mater.* **2014**, *365*, 83-87.
55. Waseda, Y.; Matsubara, E.; Shinoda, K. In: *X-Ray Diffraction Crystallography*; Waseda, Y.; Matsubara, E.; Shinoda, K., Eds. Springer-Verlag: Berlin, Germany, 2011, pp. 107-167.
56. Bao, S. J.; Li, C. M.; Guo, C. X.; Qiao, Y. *J. Power Sources* **2008**, *180*, 676-681.
57. Andreev, S. V.; Bartashevich, M. I.; Pushkarsky, V. I.; Maltsev, V. N.; Pamyatnykh, L. A.; Tarasov, E. N.; Kudrevatykh, N. V.; Goto, T. *J. Alloys Compd.* **1997**, *260*, 196-200.
58. Khan, M. H. R.; Hossain, A. K. M. A. *J. Magn. Magn. Mater.* **2012**, *324*, 550-558.
59. Nyamen, L. D.; Rajasekhar Pullabhotla, V. S.; Nejo, A. A.; Ndifon, P.; Revaprasadu, N. *New J. Chem.* **2011**, *35*, 1133-1139.

Electronic supplementary information



Scheme S1. Preparation of *N,N'*-bis (5-methoxybenzaldehyde)-4-methylorthophenylenediimine **2** and the corresponding Co(II) complex **4**.

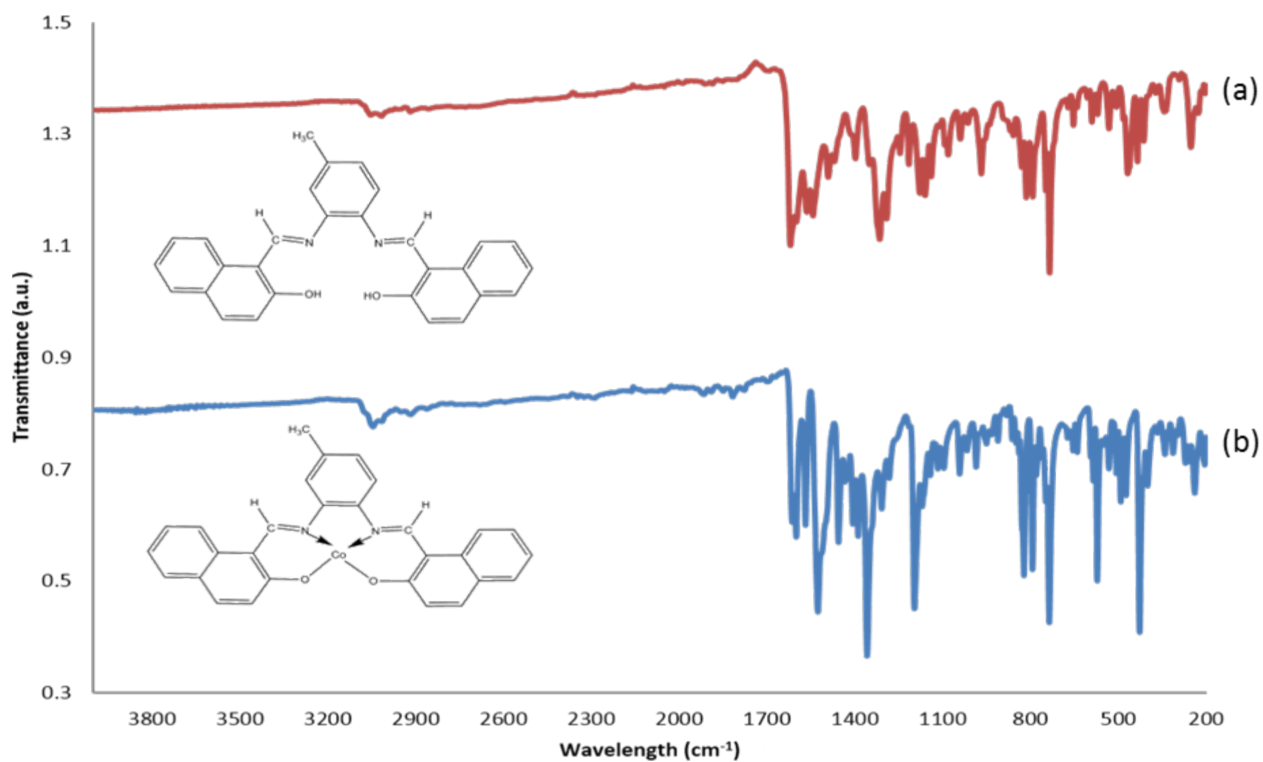


Figure S1. IR spectra of Schiff base (a) ligand **1** and (b) complex **3**.

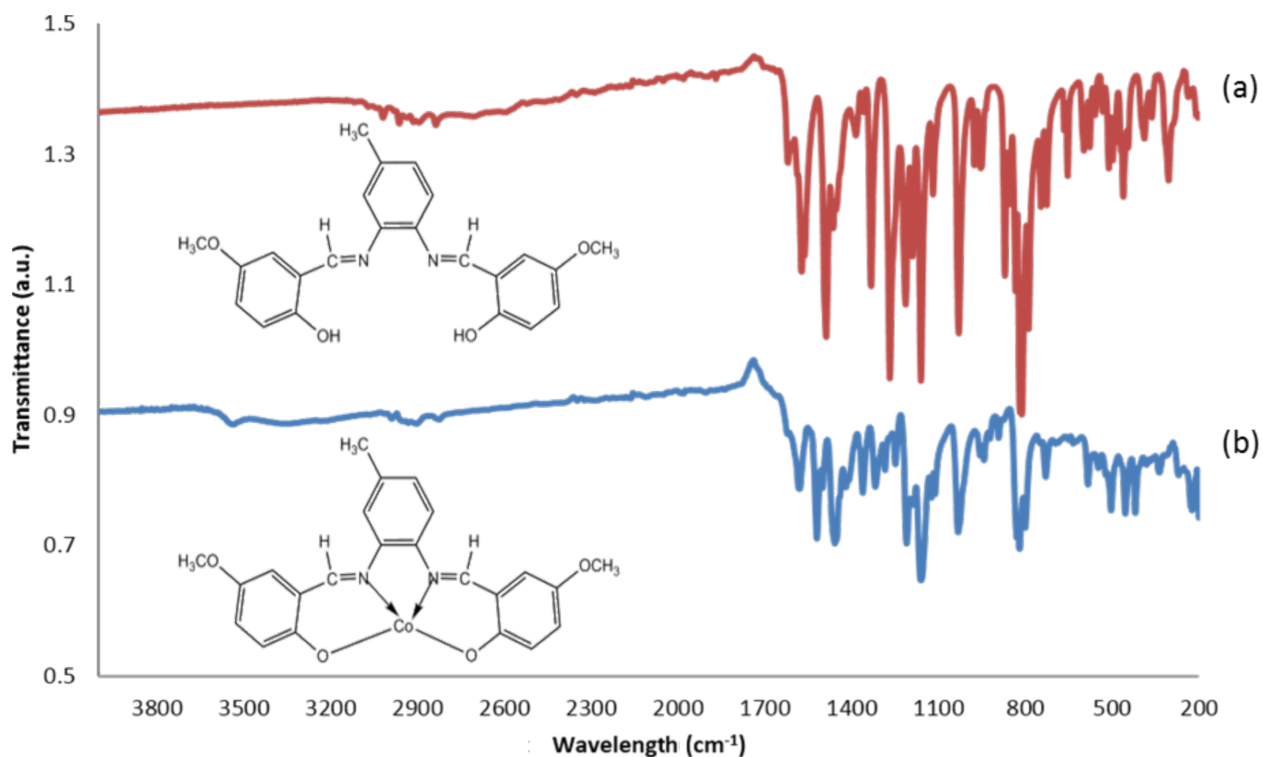


Figure S2. IR spectra of Schiff base (a) ligand **2** and (b) complex **4**.

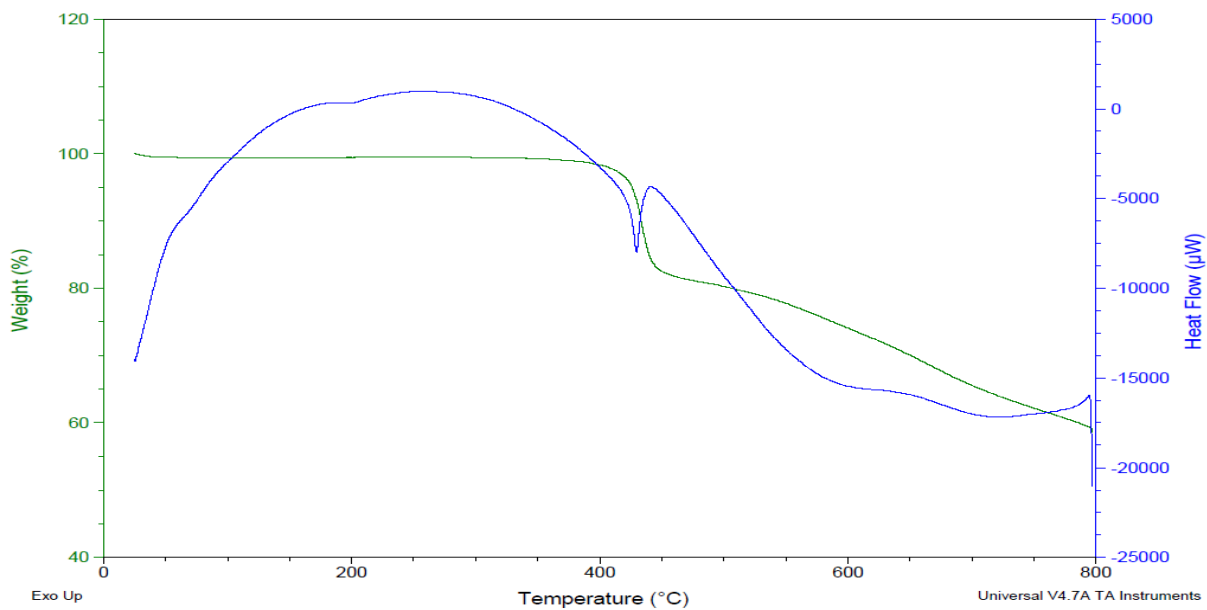


Figure S3. The TGA (green) and DSC (blue) thermogram of complex **3**.

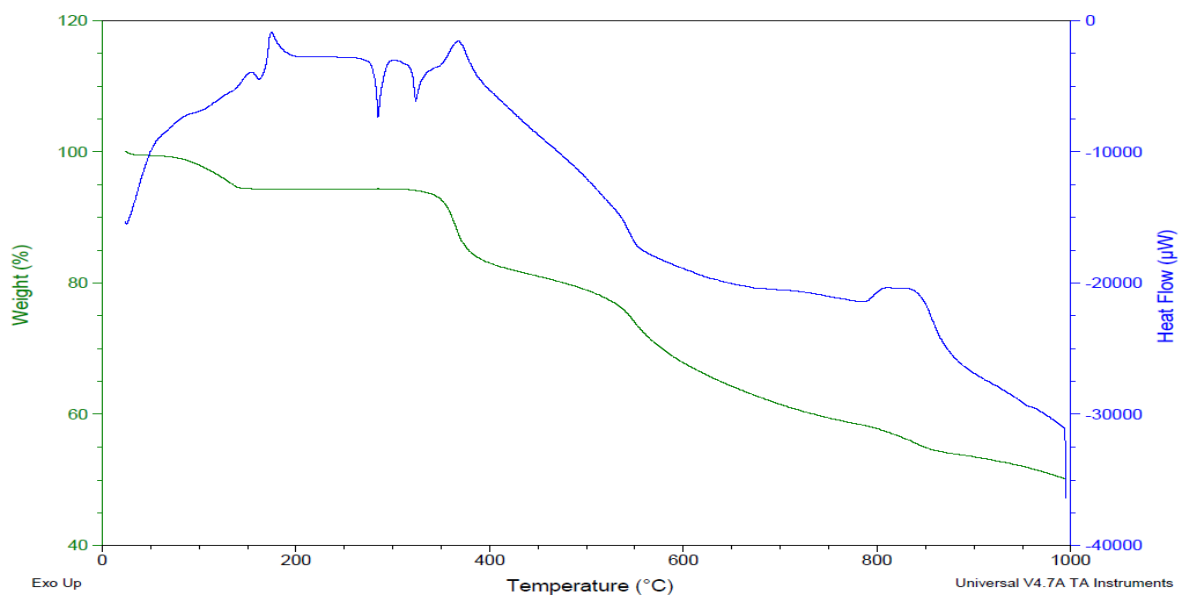


Figure S4. The TGA (green) and DSC (blue) thermogram of complex 4.